Journal of Coastal Research	37	5	933–945	Coconut Creek, Florida	September 2021

Development of a Highly Portable Unmanned Surface Vehicle for Surf Zone Bathymetric Surveying

Holly Francis[†] and Peter Traykovski[‡]*

[†]Mechanical Engineering
Stanford University
Stanford, CA 94305, U.S.A.

[‡]Department of Applied Ocean Physics and Engineering
Woods Hole Oceanographic Institution
Woods Hole, MA 02543, U.S.A.

www.cerf-jcr.org

www.JCRonline.org

ABSTRACT

Francis, H. and Traykovski, P., 2021. Development of a highly portable unmanned surface vehicle for surf zone bathymetric surveying. *Journal of Coastal Research,* 37(5), 933–945. Coconut Creek (Florida), ISSN 0749-0208.

This study reviews the design and subsequent effectiveness of a prototype autonomous survey vehicle built to collect data specifically in the surf zone. The breaking wave transitional zone between ocean and land is an important location to survey due to its impact on human infrastructure and vulnerability to the effects of climate change. However, this environment is notoriously difficult to survey due to its shallow depth and the turbulence of waves and currents. Three distinctive design choices were made at the beginning of the project with the goal of operating in the surf zone: First, the surface vehicle is light (15 kg) and fast (up to 7 m/s), both characteristics intended to enable one person to deploy it quickly and easily into the surf zone. Second, an electric motor that is connected to a jet drive eliminates a combustion engine's air intake, which can be contaminated with seawater and sand. The jet drive also removes any danger of spinning propellers and allows the vessel to run in very shallow water. Finally, the vessel has a foam bulb hatch cover that is watertight and allows the vessel to right itself if capsized by a wave. The outcome of this development effort is an unmanned vessel that has the maneuverability and power sufficient for surf zone operations and is self-righting. It runs off the waypoint based Ardupilot Mavlink program, which allows rapid transitions from autonomous modes to remote controlled modes and has a runtime of approximately 1.5 hours. The vessel has initially been used with a single beam echosounder and precision GPS to create highly detailed shallow water bathymetric maps. This study demonstrates this technique as a highly efficient method of creating bathymetric maps in coastal environments.

ADDITIONAL INDEX WORDS: *Surf zone bathymetry.*

INTRODUCTION

The surf zone is the constantly evolving transitional area between ocean and land that is characterized by high energy breaking waves. Changing coastlines often have adverse effects on the people and ecology in the vicinity; therefore, understanding this zone and how it changes is an important focus of many coastal oceanographers. Particularly as climate change continues to alter natural patterns, the impacts on human and ecological interests will only increase, directly affecting those who live along the ocean and indirectly affecting those reliant on groundwater in danger of becoming salty, roads at risk of being washed away, or other coastal aspects within reach of the ocean. Despite its widespread social relevance, data collection in the surf zone is challenging—especially for any sort of autonomous vehicle—and therefore these volatile, breaking wave environments remain very difficult to forecast or understand.

Bathymetric surveying is one common technique for understanding nearshore dynamics. The most commonly used methods to survey the surf zone bathymetry usually involve personal watercrafts (also known as Jet Skis [Dugan *et al.*, 2001]). These systems can be difficult to launch into the surf zone (especially when waves are very energetic), often requiring a large number of personnel, and have significant safety issues in rough conditions. In some locations, such as many U.S. National Park sites, their use is prohibited. Specialized amphibious vehicles have also been used but are limited to sites where these vehicles are available and are expensive to maintain and operate (Birkemeier and Mason, 1984). With the advance of tools such as robotic boats (Caccia, 2006; Manley, 1997; Manley *et al.*, 2000), seafloor crawlers (Crandle, 2017), and unmanned aerial vehicles (UAVs) (Gonçalves and Henriques, 2015; Long *et al.*, 2016), tasks like creating topographic and bathymetric maps have become much less expensive both in time and money. However, the surf zone is challenging for these types of technologies because of the chaotic, energetic nature of breaking waves. Shallow water and waves cause problems for robotics that are traditionally more suited for the open ocean or protected coastal areas such as harbors or estuaries.

This project was inspired primarily by the Woods Hole Oceanographic Institution's Jetyak, a kayak modified for oceanographic research with a jet drive motor and autonomous capabilities (Kimball *et al.*, 2014). This vessel is highly versatile and is a lower cost solution to conduct research in larger, shallow environments such as estuaries, as well environments dangerous to manned expeditions such as alongside glaciers. However, the Jetyak requires a minimum two people to deploy with either a crane or a trailer, or three people without mechanical lifting aids, which are often unsuitable for surf zone deployments. It is gasoline powered, with an air intake that is vulnerable to water infiltration. It has a maximum speed of 6

DOI: 10.2112/JCOASTRES-D-20-00143.1 received 5 October 2020; accepted in revision 20 March 2021; corrected proofs received 25 May 2021; published pre-print online 17 June 2021.
*Corresponding author: ptraykovski@whoi.edu

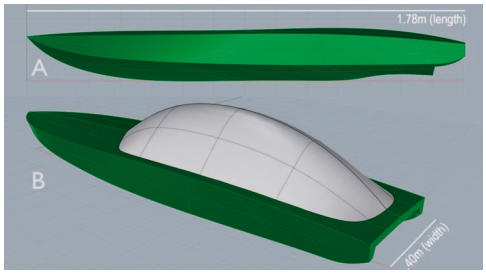

Figure 1. (a) 3D model of just the hull, imported into the 3D modeling software Rhino using photogrammetry. Note the flat top, which results in the vessel being stable upside-down as well as right-side up, an issue for a vessel that might be flipped by a breaking wave. (b) 3D model of the hull with the added flotation on top; this is the final version of the vessel and is self-righting.

knots (3 m/s) and struggles to navigate in waves larger than 30 cm in the surf zone.

Perhaps the closest existing design to a wave capable unmanned surface vehicle (USV) is the emergency integrated lifesaving lanyard (EMILY) by HydroNalix. This small, fast, remote controlled and autonomous vehicle was designed as a life saving device. The vessel is small enough to be deployed easily and quickly by one person and powerful enough to drive through breaking waves to reach a victim. The vessel has flotation on top which not only provides aid to the swimmer, but also allows the vehicle to be self-righting. The EMILY is 1.4 m long, electric, and can run for short periods of time at 25 knots (12 m/s). This design is the closest to what might be required by a surf zone research vessel, and motivated choices in the design presented. Equipped with a single beam echosounder and sidescan sonar, the EMILY has also been successfully used for bridge scour monitoring (Schroeder *et al*., 2019). Other unmanned surface vessels have been designed for use in rough sea states, such as the articulated catamaran wave adaptive modular vessel (WAM-V) design; however, catamarans typically are not self-righting and are not suitable for surf zone usage unless the wave height is small compared to vessel size (Pandey and Hasegawa, 2015).

The goal of this project was to design a small surface vehicle that can autonomously retain control even in a high energy environment. One of the primary goals of the design is to develop a vessel that can operate in conditions where the vehicle length is comparable to wave height as this fits a niche of easy deployment in the surf zone, and suitable seakeeping characteristics in moderate wave energy conditions (wave heights of 1 to 2 m). This paper details the design and specifications of a prototype vessel and its success in mapping the surf zone.

METHODS

The hull of the prototype vessel was adapted directly from a commercially available deep-v planing remote control motorboat design (178 cm long by 40 cm wide CRC SV43, which is an approximately 1/8 scale model of an Outerlimits 43 ft offshore racing boat, $500). Note that typical prices in U.S. dollars for the major components of the system are included in parentheses. The carbon fiber lamination of the hull has good stiffness to weight ratios and allows easy modification of the hull by cutting out sections and then relaminating. This is ideal for insertion and removal of sensors as survey requirements change. Three major steps were required to outfit this hull for autonomous survey according to the design requirements. First, an alternate top to the hull was constructed to allow it to be self-righting. Second, the propulsion and electronics were installed, which included removing a small section of the V-shape in the aft end of the hull as the jet drive requires a flat stern (zero-degree deadrise angle). Third, an echosounder and precision GPS were added for its first mission to make bathymetric maps in the surf zone, with space to add other sensors later in the vessel's life. The prototype vessel was designed, constructed, and then tested in numerous different survey areas and conditions.

Self-Righting Top and Stability Analysis

The three-dimensional (3D) computer aided design software Rhinoceros™ (Rhino) was used to model the hull (Figure 1a) and to design the self-righting top (Figure 1b). Orca 3D is a naval architecture plug-in for Rhino that enables analysis of hydrostatics and hull stability at different angles of heel (tilt). Using photogrammetry (with Agisoft Photoscan software), the existing hull was modeled in three dimensions through a series of stitched images and referenced measurements, and then uploaded as a mesh into Rhino (Figure 1a). With a flat, wide deck and no additional floatation, the hull was equally stable upside-down and right-side up.

Orca 3D analysis methods were used to design and simulate the benefits of a high buoyancy top (Figure 1b). Hydrostatic stability is the balance between the center of gravity and the center of buoyancy (volume of the submerged portion of the hull) that can be quantified as a measurement of the righting arm: the horizontal separation between these two opposing forces. The righting arm is a passive characteristic dependent on the relative positions of the center of gravity and center of buoyancy; in other words, if weight is fixed in the bottom of the hull and the top floats, the vessel will always automatically self-right with no dependence on a powered system, unless caught in a complex transient dynamic situation. Figure 2 shows the righting arm as the vessel heels, the heel angle on the x-axis from right-side up at 0° to upside-down at 180° of both the hull itself (Figure 2a), and the hull with a high-floatation top (Figure 2b). Note that the righting arm in Figure 2b never reaches a negative number, which indicates that there is always a force that is attempting to restore the vessel to a right-side up position. Ballast (extra weight fixed low in the hull) also improves stability. The design was calculated to allow for self-righting without ballast, but in reality the hull rights more easily with a full payload if it is fixed appropriately.

Construction Methods

The top was cut from a low density (25 kg/m^3), expanded polystyrene closed-cell foam that retains its structure and does not absorb water, using station lines to transcribe the shape designed in Rhino to a 3D object. By measuring out x-y-z coordinates at an interval of 12.7 cm (5 inches), the basic shape was cut by hand from 5.08 cm (2 inch) foam and then glued together. This shape was faired and then fiberglassed using a vacuum bagging technique which minimizes the amount of

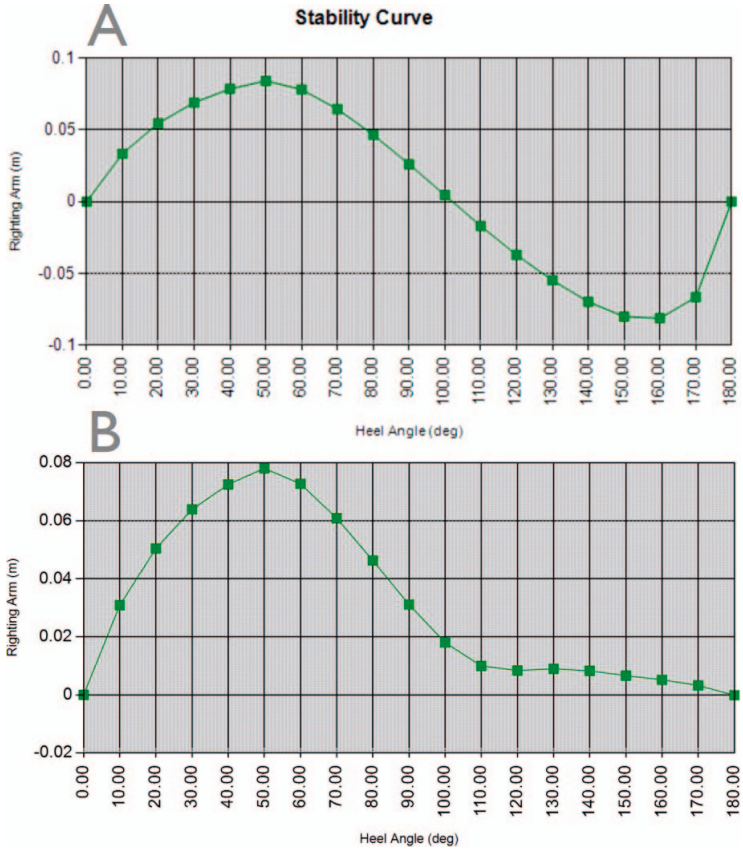

Figure 2. Stability curves for the hull (a) without self-righting lid and (b) with self-righting lid, which gives the vessel positive stability at all angles of heel. The x-axis shows the heel angle, measured as the boat rolls from upright (0°) to upside-down (180°). The y-axis gives the righting arm, which is the horizontal distance between the center of gravity and the center of buoyancy (center of submerged volume). This distance is the relevant component of the calculation of the restoring force which returns the vessel to upright. When the righting arm is positive, as it always is in (b), the vessel is returned to upright when perturbed to the given angle. If the righting angle is negative, the vessel stabilizes upside-down when perturbed to the corresponding angle. When the righting arm crosses zero, the vessel is stable at that angle.

resin used (to keep the hatch cover light) and ensures a form-fitting, smooth surface. Fiberglass was used for the lid so that radio frequency (RF) signals could transmit through the lid, unlike the carbon fiber hull which is opaque to RF transmission. A waterproof gasket was installed between the hull and hatch cover. A length of elastic shock cord was stretched across the top in numerous places, sufficiently compressing the gasket with even pressure to eliminate leakage.

Propulsion, Power System, and Cooling

A system layout is provided in Figure 3. An electric jet drive system (MHZ Model Jet 52, $400) provides both the propulsion and steering. The 5.8 kW brushless inrunner electric motor (Scorpion Model HK_5035/760KV, $350) with a water-cooling jacket is powered by two 6s (22.2 Volt, lithium polymer [Lipo]) batteries with a capacity of 13 Ah each, connected in parallel ($500). The total energy of the battery system is approximately 580 kWh (slightly variable depending on the state of final charge). The motor and speed controller (Swordfish Pro 240 Amp HV, $260) are water cooled *via* an active pumped system. A self-priming diaphragm pump is used to avoid clogging with sand. All smaller electronics are driven by a 5 V battery elimination circuit (BEC), which includes a servo for steering ($100), a radio receiver (radio control (RC), $150), a Pixhawk (autonomous control), and the water pump. The steering is accomplished with a vector thrust system on the outflow of the jet drive. This system includes a linkage to the servo, a steering shaft that passes through the transom with a waterproof seal (rubber bellows), and a small funnel. The funnel rotates, redirecting the thrust of water laterally to turn the boat.

Autonomy and Sensors

Autonomous control of the vessel was accomplished using a Pixhawk 2.1 Cube, which is a small onboard computer intended specifically for unmanned vehicle control. It communicates to a ground control station computer through a RFD 900 MHz serial telemetry radio that controls the throttle and steering systems and navigates using an onboard GPS. Typical cost for the cube, radios, and GPS is $600. The Pixhawk is controlled through the user interface Ardupilot Mavlink (Figure 4). All parameters on the vehicle's motion and control are available through this program, and new waypoints can be created and

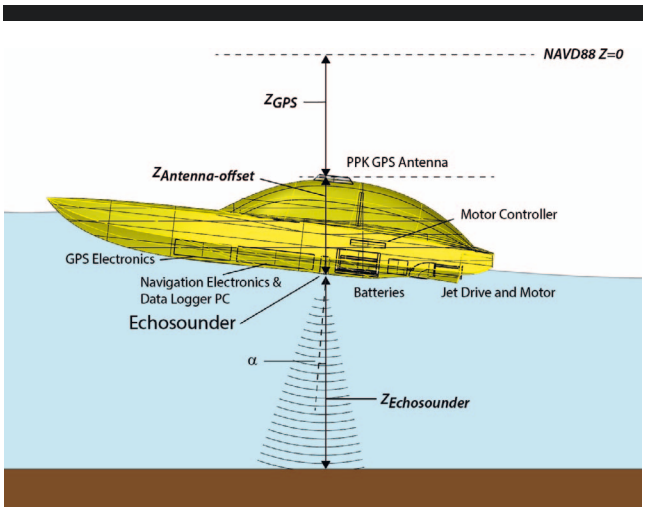

Figure 3. This schematic provides a visual summary of all electronic systems discussed and a diagram of the distances referred to in Equation (1). Three important characteristics are highlighted. First is the location of the batteries, which are the heaviest components, centered and low. Second, there is a flat section cut into the stern V for the jet drive. Third, the GPS antenna is mounted directly over the echosounder, allowing the linearity of Equation (1). In this case, $\alpha_r = 0$ because the tilt (pitch in this case) is within the half beamwidth of the echosounder. If the vessel were to tilt more dramatically, the angle would be considered in the calculation of depth. See Equation (1) for more detail.

uploaded through the telemetry in real time. The Pixhawk can either control the throttle and steering to follow GPS waypoints or can be switched into a bypass mode, which allows direct control of the throttle and steering by an operator on the beach or support boat *via* a 2.4 MHz remote control radio link ($200 for an RC radio transmitter and receiver). The autonomous steering system uses waypoint navigation, which is built into the Ardupilot/Mavlink system (Park, Deyst, and How, 2004). Since the autonomous system has no obstacle avoidance and the vessel requires careful supervision in a complex environment such as the surf-zone, it is referred to as a USV rather than an autonomous surface vessel.

An echosounder (Echologger model ECS 24 200/450 kHz) was installed directly into the hull, with a serial connection to a small windows computer (Latte Panda V1, $150) aboard the vessel for data logging (approximately $4000, but much lower cost alternatives such as the Ping Sonar Echosounder with some performance tradeoffs are now available). Software provided by Echologger is used for logging. The software also logs GPS time for synchronization with the precision GPS in postprocessing. The 450 kHz channel of this echosounder has a shorter blanking distance (depth at which the sensor cannot resolve the signal) of 15 cm, in contrast to the normal blanking distance of 50–200 cm on recreational sensors. The draft of the vessel with batteries and the echosounder is 10 cm, thus surveys can take place in approximately 30 cm minimum depth water.

While the method of using precision GPS combined with a single beam echosounder has been well established in the literature for personal water craft type vessel for nearshore survey and other larger vessels (Dugan *et al*., 2001; MacMahan, 2001) and is used widely used in commercial products (Awang and Othman, 2011; Berber and Wright, 2017; Gibeaut, Gutierrez, and Kyser, 1998), the method described here for small corrections due to tilt and transducer beamwidth is more similar to that described in the International Hydrographic Organization's Manual on Hydrography (Antoine, 2005). Dugan *et al*. (2001) also mention a simple geometric correction that appears similar though they do not provide details on the dependence of their correction on the beam pattern.

This is calculated by Equation (1):

$$D = Z_{\text{GPS}} - Z_{\text{Echosounder}} + Z_{\text{Antenna-offset}} \tag{1}$$

where, $Z_{\text{Echosounder}} = \cos(\alpha_r) R_{\text{Echsounder}}$ and $Z_{\text{Antenna-offset}} = \cos(\alpha) R_{\text{Antenna-offset}}$.

The range from the transducer to seafloor ($R_{\text{Echosounder}}$) is measured with a threshold detector on the returned intensity from the Echologger echosounder that is incorporated in the Echologger software. Spikes in the echosounder data are removed by the Matlab file exchange *spikeremoval* function (Solomon, Larson, and Paulter, 2001).

The factors α and α_r account for the tilt angle (α) from vertical of the vessel:

$$\alpha = \tan^{-1}\left(\sqrt{\tan^2(\phi) + \tan^2(\theta)}\right) \tag{2}$$

where, roll (ϕ) and pitch (θ) angles are measured by the Pixhawk inertial management unit (IMU). The reduced tilt angle (α_r) accounts for the beamwidth of the transducer that allows a vertical acoustic path to the seafloor can be approximated by:

$$\alpha_r = \begin{matrix} |\alpha| - s b_{1/2} & |\alpha| \geq b_{1/2} \\ 0 & |\alpha| < b_{1/2} \end{matrix} \tag{3}$$

The factor s depends on the level of the threshold detector, which detects when the vessel has tilted further than the beam width. This threshold was set to 0.9 for the Echologger system. $b_{1/2}$ denotes half a beam width. To illustrate this calculation, the approximate expression for reduced tilt angle is plotted in Figure 5. This image is overlayed on a numerical integration of the projection of the full beam pattern of the transducer on a flat seafloor. Two frequencies are plotted to illustrate the effect of beam width; threshold-based bed detection is included for both frequencies plotted. For the 200 kHz frequency, the correction with the reduced tilt (α_r) is quite different from the actual tilt angle (α) since $b_{1/2}$ is 5 degrees. For the 450 kHz frequency with $b_{1/2} = 2.5$, α_r is similar to α.

Given that the roll is usually less than 10 degrees, the correction for the lower frequency is usually small since $\alpha_r = 0$ for most tilt angles, and results in depth estimates that are approximately 10 to 15 cm shallower in 2 to 4 m water depths during periods of maximum roll (as will be discussed further in the results section on roll dynamics). For surveys in rougher conditions, it is generally better to use the lower frequency option due to its wider beamwidth and, therefore, less of a correction required for tilt. For calmer conditions, and particularly in very shallow water, the higher frequency is better due to its shorter blanking distance of 0.15 m (as opposed to 0.5 m for the lower frequency).

Figure 4. User interface of Mavlink, the program used to control the Ardupilot autonomy and track generation. This screen shows the display of the ground control station when the vessel is running a survey mission; in this case, a survey completed in Great Sippewissett estuary. This image provides a sense of what it is like to work with the vessel during a survey, including the map of the desired track, the actual vessel position, and relevant numbers such as distance to waypoint and vessel speed.

By pairing the sonar readings with data from a precision GPS (postprocessed kinematic [PPK] differential GPS) (Z_{GPS}), the vessel is able to make detailed bathymetric maps of shallow areas in the surf zone. The waterproof GPS Antenna (Javad AirAnt) was mounted outside the lid for minimum signal distortion and data is logged internally on the Novatel OEM-V2_L1/L2 at 10 Hz for PPK processing with Novatel Inertial Explorer software.

The measurement of the seafloor depth relative to a GPS derived vertical datum is independent of the position of the water surface. The processing defined by Equation (1) accounts for vertical fluctuations in boat position due to tides, longer

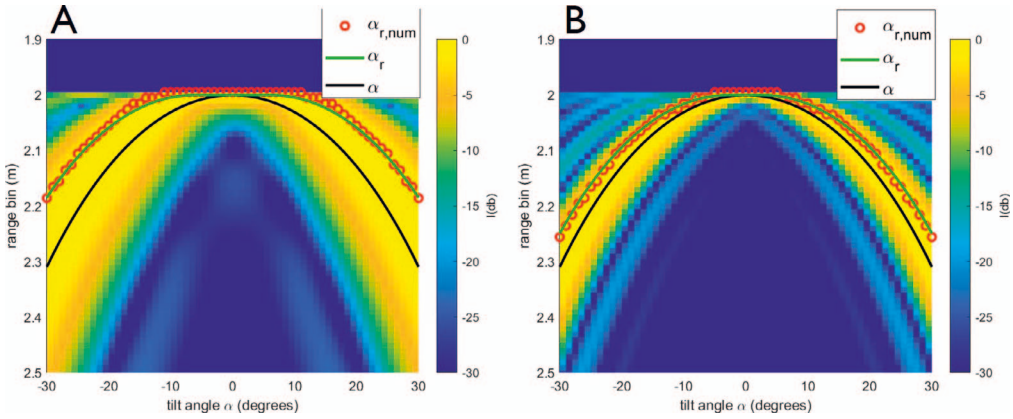

Figure 5. The approximate expression for α_r (green line) and α (black line), overlayed on numerical integration of the beam pattern intensity projection (color scale) on a flat seafloor. All calculations were completed using an example distance of 2 m from the transducer. The x-axis shows the tilt angle of the echosounder and the y-axis shows the range. The range is determined from a threshold detector on the numerical results (red dots). The echosounder frequencies are (a) 200 kHz and (b) 450 kHz.

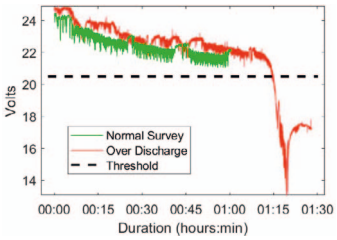

Figure 6. Battery life during two different survey runs. A standard run is compared to a run during which the batteries were overdrawn. A dashed line shows the advised minimum voltage.

term water level changes, and waves. Thus, no additional data on the water surface level, such as a tide gauge, is required. In addition to bathymetry, the GPS measurements track the water surface, allowing estimation of wave height. The wave band filtered ($0.05 < f < 1$ Hz) range to seafloor ($R_{\text{Echosounder},w}$) is highly correlated to wave band fluctuations in $Z_{\text{GPS},w}$ with typical r^2 values of 0.6 to 0.8. Thus, processing with Equation (1) in energetic wave conditions (wave height of 1.2 m as estimated by $4\sigma_{Z_{\text{GPS},w}}$, where σ is standard deviation) reduces the wave band filtered depth standard deviation ($\sigma_{D,w}$) by a factor of 3 to 4 relative to $\sigma_{R_{\text{Echosounder},w}}$.

RESULTS

Since the construction of the vessel in summer of 2018, it has been used in seven different research project-related surveys and numerous smaller testing, demonstration, and educational activity related operations. Here, the general performance of the vessel is presented, followed by the results of two surveys to demonstrate the capabilities of the vessel.

Vehicle Performance

Initial testing focused primarily on self-righting ability (stability), endurance (battery and motor characteristics), track error (steering accuracy), and roll dynamics (the effect of vessel motion on survey results).

Self-Righting Ability

To date, the self-righting ability was only formally tested in hydrostatic conditions. When flipped upside-down manually, the vessel rolled rapidly to right-side up due to the high floatation of the bulb and weight of the ballast. When in operation, it would require powerful, plunging waves to flip the vessel upside-down momentarily. While the vehicle has been deployed in spilling breakers up to 1.5 m height, it has not yet been deployed in consistently plunging breakers. The vessel has, however, been launched in conditions with plunging swash breakers. In these conditions, the vessel is manually controlled to rapidly accelerate out of the swash and then returned to survey mode, without surveying the swash region. The self-righting dynamics are essential in a boat designed to work in the surf zone to account for the rare occurrence of a capsize, as this failure mode would otherwise have catastrophic consequences, perhaps leading to loss of the vessel. The conditions where a capsize is possible are also the most difficult to recover the vessel by other means. It is worth noting that this self-righting feature is purely a physical, static equilibrium characteristic and is not dependent upon any powered system. When navigation is possible, the performance dynamics that typically effect survey results are track following error and initial roll stability at small roll angles.

Endurance

Runtime is dependent on the type of mission, the speed at which the mission is run, and the sea state. After testing was done with different weights, numbers of batteries, and at different speeds, this study can comment generally on the power performance of the vessel. The vessel was typically run with two 22.2 V, 13 Ah batteries in parallel. In initial testing, BECs (Battery Eliminator Circuit DC converters, typical 24 to 5 V) with current sensors were added to one of the batteries as the BEC was not rated for the current that could be drawn by the entire system. According to these initial measurements, the vessel drew an average of 7.3 amps from one battery over 10 minutes, with an average speed of 3.1 m/s; the highest currents of 40 amps occurred when the vessel was accelerating from a standstill. Thus, the runtime at this speed should be $13\text{Ah}/7.3A = 1.8$ hours. These tests were performed before the echosounder and data acquisition system were installed, which add drag and additional power consumption.

Though the current sensors were removed after initial testing due to excessive heat generation, the voltage is communicated through telemetry to the Mavlink system and can be used as a proxy to understand battery capacity. This measurement is carefully monitored, and the mission is aborted if the batteries approach 20.5 V, at risk of permanently damaging the batteries.

Figure 6 shows two examples of voltage readings as two batteries run from full charged to nearly empty at survey speeds of 2.5 m/s, with occasional higher bursts. The dip at the end of the overdrawn scenario occurred when the batteries were depleted, overheating, and no longer able to manage the demand of current. Though this type of use is not recommended for the long-term health of Lipo batteries, it was educational to understand their limitations. The typical run time of the vessel with the two 22.2 V, 13 Ah batteries in parallel ranged from 1:10 to 1:20 hour:min in actual field operations.

Track Error

Track error is automatically calculated and stored in the Ardupilot program. Using the documented error (distance from desired track), the effectiveness of steerage in different conditions was analyzed. As a qualitative analysis, it was apparent that the vessel was more successful in staying on course on calm, windless days with little current and plenty of space to make large turns versus a windy, wavy day with current and tight turns. It is worth noting that track error and deployment logistics were the limiting factors for wave size, not stability. The vessel was much more likely to encounter problems staying on the track than with being flipped over. Figure 7 shows a survey conducted at Long Point, Martha's Vineyard (Massachusetts) in ideal conditions: plenty of space, weak currents (less than 20 cm/s), and a moderate height ($H =$ 0.5 m) long period (peak period, $T_p = 11$ s) swell that broke intermittently with the largest waves sets on an offshore sand bar during the high tide conditions when the survey was

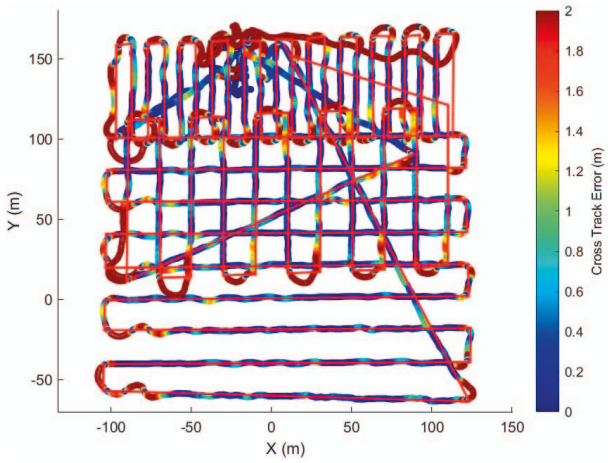

Figure 7. Ideal track following at Long Point on Martha's Vineyard. The desired track is shown in red, and the line in color scale shows the actual track of the vessel, with the color scale denoting the track error. This is an example of ideal track following, with an average cross track error of 1.5 m (mostly at the turns) with minimal oscillation along the grid lines.

performed. The average cross track error in this case was 1.5 m in waypoint following mode. Most of this error was near turns. The error on long straight sections was typically less than 1 m. This does not include the brief periods during which the vessel was switched to remote control mode to proactively avoid intermittent breaking waves. In contrast, Figure 4 shows a survey done inside Great Sippewissett estuary (Massachusetts), which has tidal current as well as limited space for the vessel to turn. The 4 m track line spacing within the estuary required staggered lines to minimize oscillation at the beginning of the line. The average error in this more difficult case was 3.3 m.

Roll Dynamics

In order to examine the small angle roll stability during survey conditions (as opposed to large angle roll stability during capsize conditions), roll measurements from the IMU of the Pixhawk were compared to wave measurements from the GPS ($Z_{GPS,w}$) for three surveys. The roll measurements (φ) or the magnitude of roll ($|\varphi|$) was directly correlated to $Z_{GPS,w}$, with an r^2 of less than 0.1. Filtering the time series of $Z_{GPS,w}$, and φ with a sliding 60 second window standard deviation and correlating these two quantities also resulted in low correlations ($r^2 \sim 0.1$) as the $Z_{GPS,w}$ fluctuations are dominated by long period swell ($T = 8$–10 s), which do not induce roll. However, if only the high frequency waves are considered by adjusting the filtering band to $0.3 < f < 4$ Hz (using the same sliding standard deviation window) the correlations increase to $r^2 \sim 0.5$. The output of the sliding standard deviation filter for high frequency wave height ($4\sigma_{SW}$, $Z_{GPS,hpw}$) is plotted against the sliding standard deviation filtered roll $\sigma_{SW,\varphi}$ in Figure 8 for three surveys. This processing captures periods of small waves and large waves at the wave group (or set) time scale during an individual survey and compares the fluctuations in roll during a 60 second window to high frequency waves in the same window. The Great Sippewissett survey took place in very

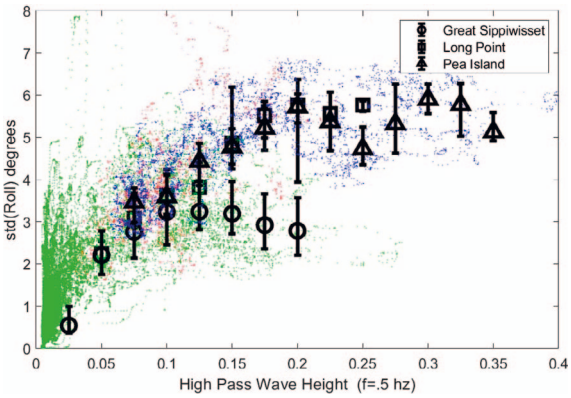

Figure 8. Roll dynamics from three different surveys. $\sigma_{SW,\varphi}$ *vs.* $4\sigma_{SW}$, $Z_{GPS,hpw}$ for Great Sippewisset (green dots and circles), Long Point (red dots and squares), and Pea Island (blue dots and triangles). The small dots are the raw data, and larger symbols represent the median in bins of 0.2 ($4\sigma_{SW}$, $Z_{GPS,hpw}$) width, the upper and lower error bars indicating the 25th and 75th percentile of the data in each bin.

small waves ($H = 0.2$ m, $T_p = 4$ s), while the Long Point survey occurred in slightly larger waves ($H = 0.6$ m, $T_p = 11$ s), and the Pea Island, North Carolina survey occurred in the most energetic conditions ($H = 1.2$ m, $T_p = 9$ s). Both of the open ocean surveys (Pea Island and Long Point) occurred in light winds, and thus high frequency wave heights were small (less than 40 cm). For all of the surveys, the roll fluctuations increase with increasing high frequency wave height, and then level off as is shown in Figure 8. For the Great Sippewisset survey in small waves, the $\sigma_{SW,\varphi}$ levelled off at 3 degrees (within 1/2 beam width of the echosounder). In this very shallow survey, with small amounts of tilt, the 450 kHz frequency was used due to its reduced blanking distance. For the open ocean surveys at Long Point and Pea Island in more energetic conditions, the $\sigma_{SW,\varphi}$ levelled off at 6 degrees, and thus the lower, wider beamwidth frequency was used. These surveys were generally in depths of greater than 1 m, so the blanking distance was not an issue. The region shallower than 1 m near the beach were in the swash zone and had plunging or steeply surging waves in which the vehicle could not survey consistently.

Measurement Accuracy Evaluation

To assess the altitude measurement accuracy of the combined GPS, echosounder, and USV system relative to the Geiod, two controlled tests were conducted in a calm (wave height less than 15 cm) water environment with a gently sloping (4/100) sandy seafloor with small (height –0.02 cm, wavelength +10 cm) ripples. A Javad Triumph 2 L1/L2 precision Global Navigation Satellite System receiver was mounted on a 4.3 m mast. On the first day a single person held the mast with one end on the seafloor at 12 stations for 15 seconds at each station, with depths ranging from 1 m to 4 m. On the second day, using a two-person kayak with one person ensuring the mast remained vertical, 16 stations were occupied for 30 seconds each. The USV was towed behind the kayak during the GPS-mast survey. Immediately after the GPS-mast survey the USV was programmed to conduct a waypoint

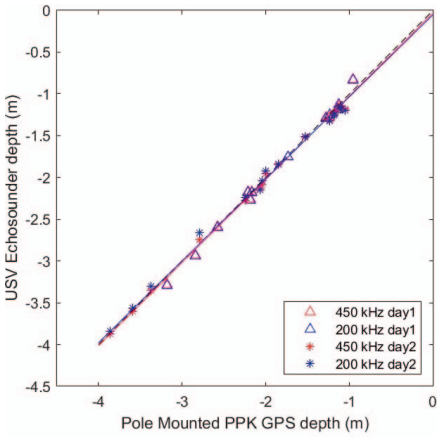

Figure 9. This figure shows the high correlation between a pole-mounted GPS measurement of depth and the USV echosounder depth, both relative to the same NAVD88 reference. Data for both the 200 kHz (blue) and 450 kHz (red) echosounder channels are shown with the best fit results as a solid line of the same color. The triangles are data from the first survey day and the asterisks are from the second day.

mission at the locations where the mast stations took place. Both the GPS on the USV and the mast rover were processed in PPK mode relative to a base station within 200 m of the furthest mast station. The mast data was averaged over the period of station occupancy and the USV GPS data was used to search for times when the vehicle was within a specified range of each station.

It was found that a search radius of 2 m gave the least root mean square (RMS) error between the USV depth estimate and the mast depth estimate. A very small search radius (less than 1 m) led to no USV data as the USV did not always go exactly over all the mast stations. With a slightly larger search radius, no stations were missed but some had lower numbers of echosounder samples to average. The agreement between the USV depth measurements and the mast measurements is excellent. The RMS errors between the two measurement is just slightly larger than the combined manufacturer specified vertical accuracy of each GPS of 1.5 cm each (Figure 9). The RMS error of the 450 kHz echosounder measurements versus the mast measurement with the data from both surveys was 5.6 cm and the RMS error of the 200 kHz measurements was 6.7 cm. The slope and intercept of a best fit line for the 45 kHz was (0.996, –0.03) with a 0.99 r^2 value. The 200 kHz slope and intercept were (0.98, –0.05), also with a 0.99 r^2 value.

Surveys

The first survey took place in Great Sippewissett Tidal Estuary (Valiela, 2015) in Falmouth, Massachusetts as part of a graduate student project to learn how to integrate and compare bathymetric data from the USV with topography and bathymetry data acquired from a multirotor unmanned aerial system (UAS). This survey took place in a very shallow tidal estuary (0 to 1.5 m depth) and is the only survey performed where there is a second source of bathymetry data to compare with the USV results. The second survey took place on Long Point in Martha's Vineyard and documents the ability of the vessel to perform surveys in a beach exposed to open ocean swell and took place before and after a 4 m wave height event with significant sandbar migration.

Great Sippewissett Tidal Estuary, Massachusetts: A Comparison to Other Survey Methods

The Great Sippewissett estuary was mapped using both the USV and an aerial drone (Figure 10). The drone survey was done using a photogrammetric structure from motion techniques (similar to the structure from motion [SfM] methodology from Gonçalves and Henriques [2015] and Long *et al*. [2016]) based on images taken with a DJI Martice 200 UAS equipped with a DJI Zenmuse x4s camera system and a Loki PPK GPS system flown at both 30 and 60 m above sea level. The GPS system can record the location of the camera within 3 to 5 cm, and combined with 10 PPK GPS surveyed ground control point (GCP) marker flags results in topographic accuracy of 5 to 10 cm on land. The SfM processing was conducted in Agisoft Metashapes software. The accuracy was assessed by using five of the GCPs in the solution as control points and retaining five independent GCP markers as check points. All vertical measurements were referenced to North American Vertical Datum of 1988 (NAVD88) and horizontal measurements are in Universal Transverse Mercator (UTM) zone 19N, referenced to North American Datum of 1983 (NAD83 [National Spatial Reference System, 2011]). The UTM coordinates are shifted by $x = x_{\mathrm{UTM}} - 3,629,818$, and $y = y_{\mathrm{UTM}} - 4,604,243$ for ease of viewing. Although the topographic data could be exported at 10 cm resolution, a 50 cm output resolution was selected to match the bathymetric processing. The water was relatively clear, and the water surface was free from texture due to the low wind and wave conditions. This surface state combined with strong texture on the seafloor from bedforms, rocks, shells, and vegetation, led to the SfM software finding feature matches in depths of up to 1.5 m below the sea surface. Processing this data results in an apparent bathymetric surface (z_A) that is shallower than the true bathymetric surface (z_0) due to refraction of the optical rays at the air water interface (see Figure 11 for a diagram of terms). The apparent bathymetry (z_A) can be corrected for the effects of refraction *via* Equation (4).

$$z_0 = \alpha(z_A - h_w) + h_w \tag{4}$$

The refraction correction term $\alpha = h_0/h_A$ refers to the relation between the apparent depth (h_A) and the actual depth (h_0). The water level (h_w) can be found from linear regression of z_A with the true bathymetry (z_0) measured with the single beam echosounder on the USV. The water level can also be found from the SFM topography by examining the vertical location of the waterline. Both of these methods find similar results. The value found in these measurements of $\alpha = 1.49$ is consistent with other measurements made using the same aerial system (in the range of $\alpha = 1.42$ to 1.56), but with a more refined bathymetric measurement system based on a PingDSP 3DSS bathymetric sidescan sensor coupled with a Novatel IGM IMU-A1 Dual PPK GPS attitude position reference system on the Jetyak USV (Traykovski, Sherwood and Ralston, 2018). The Jetyak measurements were performed in the Nauset Estuary in

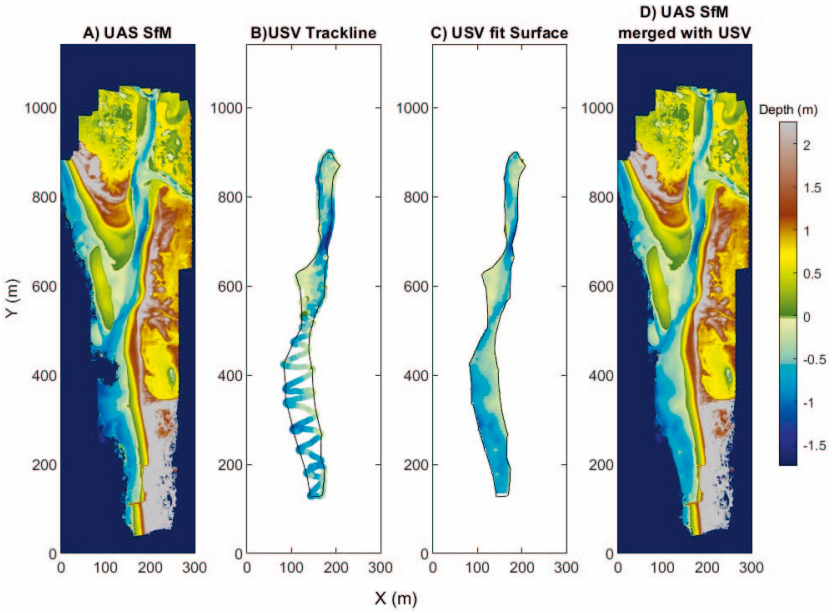

Figure 10. Great Sippewissett tidal estuary. Comparison and merging of drone mapping technique with the surface vessel's mapping results. (a) Shows the UAS map. Note the gaps in deeper water. (b) Shows the actual vessel path, completed using a combination of autonomous waypoint following and manual remote control to explore the edges of the estuary, which were not known before the survey. (c) Shows interpolation of the USV data from (b). Finally, (d) shows the integration of both sets of data into a full map of the estuary. See Figure 12 for correlation between the datasets.

Orleans and Eastham, Massachusetts, which has a typical tidal range of 2 m. Thus, in addition to comparing SfM refraction corrected bathymetry to *in situ* Jetyak based bathymetry, some data comparison of SfM subaerial topography and Jetyak bathymetry was possible to confirm the accuracy of the technique by performing SfM surveys at low tide and bathymetric surveys at high tide similar to methods reported by (Genchi *et al*., 2020). More detailed approaches involving correction to each matched feature to correcting SfM bathymetry are available but were not justified for this work given the computation expense and other sources of error in comparing SfM based bathymetry to echosounder data, such as bedform migration or other topographic change between surveys.

The bathymetric survey with the USV was performed using a combination of waypoint following autonomous modes to run parallel paths 4 m apart and manual remote control steering to closely follow the channel banks, whose precise location was not known before the survey. The PPK GPS data was used to reference the echosounder data to a NAVD88 vertical datum and horizontal NAD83 horizontal datum. The irregularly spaced track line data was interpolated onto to a regular 50 cm grid using the Matlab file exchange function Regularize-Data3d (Jamal, 2014), and the Matlab function boundary to find the convex hull of the track line data points so the data is only interpolated and not extrapolated (Figure 9b,c). For the final combined bathymetric and topographic map, the data points in the SfM survey were replaced by interpolated points from the echosounder survey within the convex hull of the echosounder track lines. A 1.5 by 1.5 smoothing filter was applied to the final surface to remove any sharp transitions between the two processing methods.

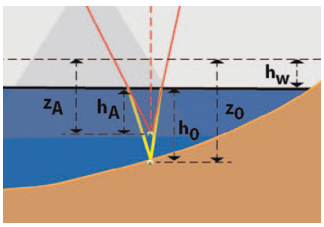

Figure 11. Geometry of the optical refraction at the air water interface. This technique is used to correct SfM derived bathymetry and is relevant as a comparison to the USV echosounder measurements.

Refraction corrected SfM data was also interpolated onto the track line of the echosounder to compare the two methods (Figure 12a,b). The two methods produce very similar results that are highly correlated ($r^2 = 0.96$) as both methods follow the structure of the topography well. The mean of the difference is zero due to the refraction correction method and the 25th and 75th percentile of the difference are –0.9 and 2.6 cm, respectively. The RMS error is 4 cm.

Long Point Ocean Beach, Martha's Vineyard: Pre- and Post-storm Bathymetric Surveys

The second survey highlighted here involved repeat mapping with a five-day interval between surveys before and after a high energy wind and wave event in an effort to capture the

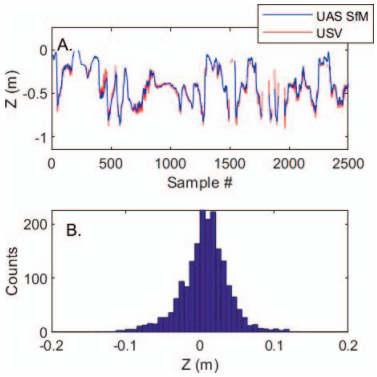

Figure 12. Great Sippewissett survey (a) comparison to an aerial drone's measurements along the track of the USV and (b) the error histogram for plot (a).

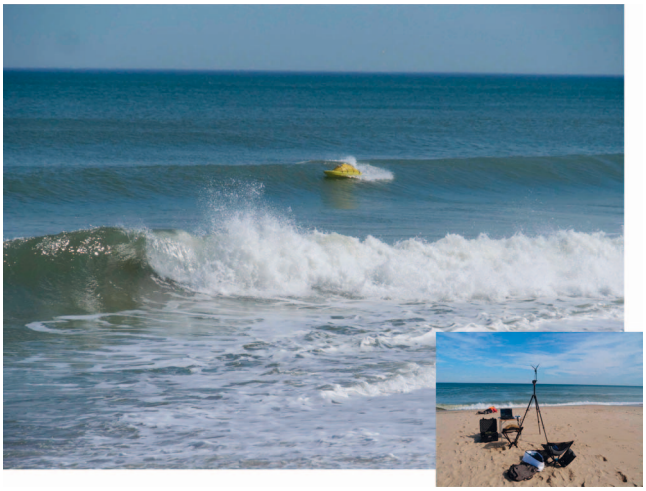

Figure 13. (Main figure) The vehicle underway conducting a turn at the near-shore end of a survey line in moderate breaking waves. (Inset figure) the highly portable control station set up on the beach within visual range of the vessel.

effects of the storm on the nearshore bathymetry. The first survey was performed on 26 October 2018 in 0.3 m significant wave height ($H_{1/3}$) at high tide; thus, very little wave breaking was occurring in the survey area, except for a small surge on the shore. The storm reached peak intensity on 28 October with $H_{1/3} = 4.0$ m, T_p (peak period) = 11 s waves that broke across the entire survey area. The second survey occurred on 31 October 2018 in $H_{1/3} = 0.7$ m, $T_p = 11$ s waves that intermittently broke in the inner part of the survey area and had a consistent surge on the shore. Due to its lightness and safe jet drive design, the vessel was easily deployed by two people. One person would place the vessel in the uprush of the surge at 10 to 20 cm depth water, and the other, on dry land, would quickly apply throttle to accelerate out of the surge zone. Once the vehicle was beyond the surge it was switched into autonomous GPS waypoint following mode. The track line consisted of shore-perpendicular lines 10 m apart near the beach to capture details of the nearshore zone (Figure 7). In regions with intermittent breaking waves, shore-perpendicular lines are better than shore-parallel lines as the vehicle deviates less from its intended course heading directly into or away from breaking waves. While tracking shore-parallel lines, if the vehicle is hit from the side by a breaking wave, it would deviate up to 10 m from its intended course. The waypoint following mission could be momentarily paused by the remote-control operator during larger sets of waves and then resumed after the waves had broken. One weakness of the autonomous mode is that when the vehicle is surfing down a steep wave face, the autonomous throttle controller reduces throttle, which reduces steering control with the vectored thrust jet drive system. Figure 13 shows the vehicle in manual RC mode accelerating across a wave under full throttle to regain steering control. This unintended surfing mode only occurs occasionally with steep waves either just before, during, or immediately after breaking, and therefore has not been found to be a significant impediment to successful surveys. The second person, who had previously launched the vessel, would be on standby for rapid redeployment if it were washed up on the beach in a surging breaker, although this did not occur during this survey. Offshore of the intermittent breaking zone, the shore-perpendicular lines were spaced by 20 m and overlapped with 20 m spaced shore-parallel lines which extended into deeper water. The beach topography (above −1 m NAVD88) was surveyed with a PPK GPS mounted on a pole strapped to a backpack and the operator would walk shore perpendicular transects approximately 10 m apart, while the vessel was surveying the offshore regions.

Figure 14 illustrates the effectiveness of this vessel in measuring sandbar migration that occurs due to the large waves and undertow flows during the storm. Before the storm, the sandbar crest was located at $Y = 115$ m, 65 m from the mean tide shoreline and had a depth of 1.3 m at the crest. While the overall mean tide shoreline position did not change significantly during this storm, a series of rhythmic oscillations, known as beach cusps (Coco, O'Hare, and Huntley, 1999; Evans, 1938), did form and the sand bar migrated out to a location of $Y = 60$ m with a depth of 2.4 m at the crest.

In addition to measuring bathymetric change during this survey, a small ultrashort baseline (USBL) acoustic receiver array (Jaffre *et al*., 2015) was installed in the vessel for these surveys to track the location of acoustic pingers which were attached to a steel cylinder to simulate the mobility of unexploded munitions from previous military training activities (Traykovski, 2020). A combined USBL and Doppler-based localization scheme was successful in measuring mobility of some of the cylinders of distances up to 10 m during the energetic storm with an accuracy of 3.8 m, before the cylinders were buried by the migrating sand bar that was also measured by the USV.

DISCUSSION

Overall, this development effort has successfully produced a surface vehicle that is well-suited for meeting the challenges of surveying in the surf zone. The vessel completes a survey track in GPS waypoint following mode, turning in a timely manner

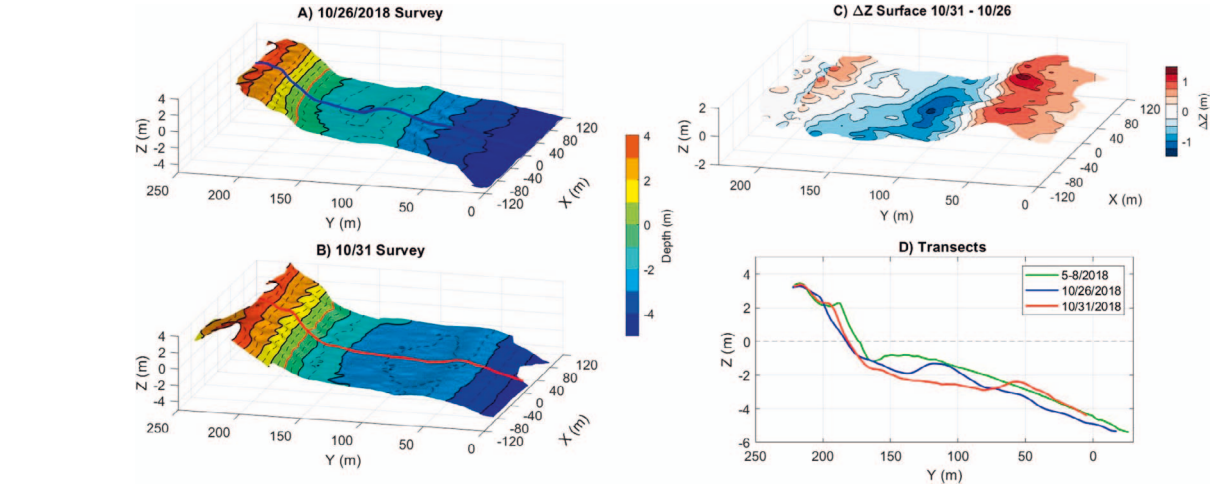

Figure 14. These paired surveys "a" and "b" were run before and after a large wave event (4 m). The vessel effectively measured sandbar migration as shown by (c) in shore perpendicular transects extracted from each survey. In (d), the blue transects show the location of the sandbar before the storm and the red transects show the location afterwards.

and traveling in a straight line, with the ability to override the autonomous mode *via* remote control if needed. It has some trouble with turning sharply if there are high winds or large waves that catch the bow, but it is generally able to overcome these challenges and return to course. The vessel is self-righting and watertight, though its watertight seal is carefully monitored. It can achieve speeds of greater than 15 knots (7 m/s) even at full payload capacity, and though this speed is generally unnecessary for survey operations, it is very useful for quickly avoiding breaking waves and other dangerous situations. The vessel has a runtime of 70 minutes during a 2.5 m/s survey with two batteries. The runtime is based on tests at a variety of speeds to full discharge of two batteries and could be extended with more batteries. Finally, the vessel is a total of 15 kg, easily deployable by one person.

Utility

This vessel improves upon the existing technology in three ways. First, the vessel is much less expensive than the majority of track-following autonomous bathymetric survey vessels. This allows for much more accessible, highly precise bathymetric surveys for use in many different fields that would normally be limited by the cost of data collection. The cost of the parts to build the boat was approximately $3500, excluding the precision GPS and echosounder. These items were several thousand U.S. dollars each, but much lower cost alternatives for several hundred dollars each that should meet the required specification are now commercially available. Second, the vessel is much safer (both for the operators and for the vessel itself) than other vessels that are larger, that use exposed propellers (compared to a jet drive), and that are not watertight and/or self-righting. This allows the vessel to be used in much broader conditions without as much concern for the safety of the operators or the risk of loss of an expensive piece of equipment. Third, the vessel is easy to use. It can be carried into the field, launched, and supervised all by one person or two people, as opposed to other survey vessels that require a trailer, a calm launching point, and a team of people. This characteristic dramatically increases the vessel's flexibility, and therefore, days on the water collecting data.

Limitations

While exact criteria that limit the successful operation of the vessel are still being determined in ongoing field work, the testing done up to this point provides a good sense of when the vessel might have difficulty completing a survey. The two primary limiting factors are wind and breaking waves. In terms of wind, the vessel tends to be blown off course when the wind is greater than 20 knots. Of course, wind also causes wind chop, which also pushes the vessel off course. These two effects are difficult to detangle (the vessel might do fine in 20 knots in a site with limited fetch, including open ocean sites with offshore directed winds), but a 20 knot wind and corresponding chop with long fetch is approximately the limit of what the vessel could reasonably handle.

The second limiting factor is breaking wave size and shape. Breaking waves due to long period swell are generally more powerful than surf from wind chop but have significantly more space between waves that allows the vessel time to recover. Long period swells also tend to arrive in groups, and depending on sand bar depth and wave height, may break intermittently and can be avoided. Successful surveys have been conducted in 1.2 m high waves which shoaled to 1.8 m height before breaking as measured by the GPS on the boat at the Pea Island site, as well as slightly less energetic conditions at Long Point. At both sites there was a steep beach with waves that were intermittently breaking on an offshore sand bar, and this region could be crossed in autonomous mode. The steep plunging swash zone (about 15 m wide) could not be consistently surveyed in these conditions. A GPS backpack could be taken on foot to within 0 to 10 m of the inside of these turns, depending on the tide at the time of the survey, leaving a small, unsurveyed gap.

In manual RC mode, quick runs into the outer swash zone were possible by timing gaps in the waves. For vessel launch and recovery, the rapid acceleration has allowed transiting the swash zone in wave heights up to 2 m. The operator only needs to wade into depths of 0.2 to 0.5 m to launch and the vessel can be run onto dry sand for recovery, which increases safety for the operator. In larger swash conditions it is expected there will be a limit where the vessel cannot make it through the waves. An additional effect of more powerful, long period swell is the whitewater between waves. Even if the turbulence does not affect the vessel's navigation, it might affect the echosounder's ability to penetrate the water column and collect meaningful data. In a surf zone with consistently breaking waves on a low slope dissipative beach, the combination of bubbles due to whitewater and navigation constraints might set a lower limit of maximum wave height than on a steep beach with an offshore sand bar. Further use in a variety of conditions will allow more precise bounds on operation limits to be set.

Design Modifications

As a prototype, this vessel has highlighted a few modifications that will be brought forward into future designs. While self-righting and powerful, this vessel still has a wave height limit of approximately one to two meters (depending on wavelength and steepness, frequency of breaking, and wind). Consistently breaking waves greater than this height push the vessel too far away from the desired course for the autonomous program to handle. In order to survey in larger waves, a second vessel that is semisubmersible is in the process of being designed. Rather than focusing on maneuverability as the primary method of retaining control in waves, a semisubmersible vessel would be more likely to pierce or "dive" underneath waves. A larger, low drag, semidisplacement hull is also under development, which will have payload capabilities to carry a small multibeam or bathymetric sidescan system.

Discussion of Effectiveness in Mapping Bathymetry

The two case studies presented in the Great Sippewissett estuary and the Martha's Vineyard Long Point before and after a storm demonstrate the capabilities of a small, versatile, autonomous research vessel such as this one. The Great Sippewissett estuary combines this technique with a UAS-based technique and shows that the two techniques produce similar and complementary results that can be used to map both dunes and near-shore bathymetry. Since the echosounder data was used to calibrate the refraction correction, this data does not establish a ground truth for the mean but does show the standard deviation of the difference between the two techniques is low ($\sim$10 cm). For this reason, a well-controlled ground truthing experiment was conducted to verify the combined echosounder and GPS system bathymetric measurement accuracy. This survey also demonstrates that the USV can map the spatial structure of a complex, very shallow system that is difficult to map with other systems due to the risk of running aground. The Long Point survey is particularly illustrative of the vessel's easy deployment and maneuverability in the surf zone and ability to efficiently measure bathymetry changes due to energetic storms. Because deployment requires only one or two people and the vessel can be hand-carried across a beach where vehicular access is unavailable, this vessel can be onsite with minimal preparation or warning, and in situations where a Jet Ski or amphibious, vessel-based systems are not feasible or efficient.

CONCLUSIONS

This vessel has proved itself as a highly efficient tool in the context of mapping high energy coastal bathymetry. By automating repetitive survey work and retaining operability in rough conditions, the vessel not only gets measurements in the surf-zone that were difficult to acquire with existing vessels, but also extends the number of field days available to a researcher because of its ease of deployment and use. With one or two people required for operation, portability, and safer operation than manned systems in the surf zone, it has the capability to increase data collection for scientists that were limited by conflicting schedules, inclement weather, and reliance on aid from technicians.

It is the hope that the vessel will be modified in the future to accommodate a larger range of small sensors. A first step in this direction was demonstrated by installing a USBL in the vessel to track mobile acoustic pingers in the surf zone. Vessels of this type may be able to play a similar role to a modern UAS, which has revolutionized topographic mapping. Aerial drone data has become applicable in many different disciplines, and it is the hope that small USVs such as this one can play a similar role in nearshore oceanography.

ACKNOWLEDGMENTS

We are grateful to our four anonymous reviewers who provided very helpful suggestions that greatly improved the manuscript. We would also like to thank David Shlimak of the U. Mass. Amherst Mechanical Engineering Department, Rachel Housego of the WHOI MIT Joint Program, Chris Sherwood of the USGS Woods Hole Coastal and Marine Science Center (cover photo), the WHOI Summer Student Fellowship staff, Stanford University professors Dr. Jeffery Koseff and Dr. Leif Thomas, the students and postdocs in COFDL, and the WHOI staff for their assistance. This project is supported by the National Science Foundation grant REU OCE-1659463, and SERDP Projects MR-2729 and MR20-1494, and Stanford University's Undergraduate Civil Engineering Research funding program VPUE SURF 2020.

LITERATURE CITED

Antoine, Q., 2005. Chapter 3 depth determination. In: *Manual on Hydrography*. Monaco: International Hydrographic Bureau, pp. 119–198.

Awang, N.A.C. and Othman, R., 2011. Hydrographic survey using real time kinematic method for river deeping. *Geoinformation Science Journal*, 11(1), 1–14.

Berber, M. and Wright, W., 2017. Hydrographic survey of a south Florida canal using a hydrolite. *Journal of Geodetic Science*. https://www.degruyter.com/

Birkemeier, W.A. and Mason, C., 1984. The Crab: A unique nearshore surveying vehicle. *Journal of Surveying Engineering*, 110(1), 1–7.

Caccia, M., 2006. Autonomous surface craft: Prototypes and basic research issues. *Proceedings of the 14th Mediterranean Conference on Control and Automation* (Ancona, Italy), pp. 1–6.

Coco, G.; O'Hare, T.J., and Huntley, D.A., 1999. Beach cusps: A comparison of data and theories for their formation. *Journal of Coastal Research*, 15(3), 741–749.

Crandle, T., 2017. SurfROVer: An ROV designed for traversing the littoral zone. *Proceedings of the OCEANS Conference* (Anchorage, Alaska), pp. 1–4.

Dugan, J.P.; Morris, W.D.; Vierra, K.C.; Piotrowski, C.C.; Farruggia, G.J., and Campion, D.C., 2001. Jetski-Based nearshore bathymetric and current survey system. *Journal of Coastal Research*, 17(4), 900–908.

Evans, O.F., 1938. The classification and origin of beach cusps. *The Journal of Geology*, 46(4), 615–627.

Genchi, S.A.; Vitale, A.J.; Perillo, G.M.E.; Seitz, C., and Delrieux, C., 2020. Mapping topobathymetry in a shallow tidal environment using low-cost technology. *Remote Sensing*, 12(9), 1394.

Gibeaut, J.C.; Gutierrez, R., and Kyser, J.A., 1998. Increasing the accuracy and resolution of coastal bathymetric surveys. *Journal of Coastal Research*, 14(3), 1082–1098.

Gonçalves, J.A. and Henriques, R., 2015. UAV photogrammetry for topographic monitoring of coastal areas. *ISPRS Journal of Photogrammetry and Remote Sensing*, 104, 101–111.

Jaffre, F.M.; Traykovski, P.; Moulton, M.; Lawson, G.L., and Austin, T.C., 2015. Development of underwater acoustic backscatter and Doppler instruments from a small and versatile multi-frequency sonar board with software defined processing. *Proceedings of the OCEANS Conference* (Geneva, Italy), pp. 1–6.

Jamal, 2021. RegularizeData3D. MATLAB Central File Exchange. https://www.mathworks.com/matlabcentral/fileexchange/46223-regularizedata3d

Kimball, P.; Bailey, J.; Das, S.; Geyer, R.; Harrison, T.; Kunz, C.; Manganini, K.; Mankoff, K.; Samuelson, K.; Sayre-McCord, T.; Straneo, F.; Traykovski, P., and Singh, H., 2014. The WHOI Jetyak: An autonomous surface vehicle for oceanographic research in shallow or dangerous waters. *Proceedings of the IEEE/OES Autonomous Underwater Vehicles (AUV) Conference* (Oxford, Mississippi), pp. 1–7.

Long, N.; Millescamps, B.; Guillot, B.; Pouget, F., and Bertin, X., 2016. Monitoring the topography of a dynamic tidal inlet using UAV imagery. *Remote Sensing*, 8(5), 387.

MacMahan, J., 2001. Hydrographic surveying from personal watercraft. *Journal of Surveying Engineering*, 127(1), 12–24.

Manley, J.E., 1997. Development of the autonomous surface craft 'ACES'. *Proceedings of MTS/IEEE OCEANS*. doi:10.1109/oceans.1997.624102

Manley, J.E.; Marsh, A.; Cornforth, W., and Wiseman, C., 2000. Evolution of the autonomous surface craft AutoCat. *Proceedings of the MTS/IEEE OCEANS Conference and Exhibition*, 408(1), 403–408.

Pandey, J. and Hasegawa, K., 2015. Study on manoeuverability and control of an autonomous Wave Adaptive Modular Vessel (WAM-V) for ocean observation. *Proceedings of the International Association of Institutes of Navigation World Congress (IAIN)* (Prague, Czech Republic), pp. 1–7.

Park, S.; Deyst, J., and How, J., 2004. A new nonlinear guidance logic for trajectory tracking. *Proceedings of the AIAA Guidance, Navigation, and Control Conference and Exhibit* (Reston, Virigina). doi:10.2514/6.2004-4900

Schroeder, B.; Haug, P.; Alvarado, A., and Baribeau, S., 2019. Unmanned surface vessels for bridge scour monitoring. *Transportation Research Board*. https://trid.trb.org/view/1641763.

Solomon, O.M.; Larson, D.R., and Paulter, N.G., 2001. Comparison of some algorithms to estimate the low and high state level of pulses. *Proceedings of the 18th IEEE Instrumentation and Measurement Technology Conference. Rediscovering Measurement in the Age of Informatics* (Budapest, Hungary), pp. 96–101. doi:10.1109/IMTC.2001.928794

Traykovski, P., 2020. *MR-2729 Rapid Response Surveys of Mobility, Burial and Re-Exposure of Underwater Munitions in Energetic Surf-Zone Environments and Object Monitoring Technology Development*. Falmouth, Massachusett: Woods Hole Oceanographic Institution, *Project MR-2729*. https://www.serdp-estcp.org/Program-Areas/Munitions-Response/Munitions-Underwater/MR-2729/MR-2729/(language)/eng-US

Traykovski, P.; Sherwood, C.R., and Ralston, D.K., 2018. Combining data from unmanned aerial systems and autonomous surface vessels to map topography and bathymetry and measure morphodynamic change in nearshore and estuarine environments. *Proceedings of the AGU Ocean Sciences Meeting* (Portland, Oregon). https://agu.confex.com/agu/os18/meetingapp.cgi/Paper/312920

Valiela, I., 2015. The Great Sippewissett Salt Marsh plots—Some history, highlights, and contrails from a long-term study. *Estuaries and Coasts*, 38, 1099–1120.